Bollettino di Geofisica Teorica ed Applicata Vol. 53, n. 4, pp. 523-537; December 2012
DOI 10.4330/bgta0060

Application of quaternion algorithms for multicomponent data analysis: a review

A. Mazzotti[1], A. Sajeva[1], G.M. Menanno[2], A. Grandi[3] and E. Stucchi[4]

[1] *Earth Sciences Department, University of Pisa, Italy*
[2] *Earth Sciences Department, Dhahran, Saudi Arabia*
[3] *TOTAL, Milan, Italy*
[4] *Earth Sciences Department, University of Milan, Italy*

(Received: April 1, 2011; accepted: March 16, 2012)

ABSTRACT In this paper we illustrate the applications of three algorithms of multicomponent seismic data processing, velocity analysis, deconvolution, and seismic wavefield separation, that we implemented by means of quaternion algebra. After a brief introduction on quaternions and a review of these methods, we focus our description on the applications to actual multicomponent seismic data sets. Quaternion velocity analysis results in an improved resolution and distinction of the velocity trends associated with the various wave phases, while the extension of the classical Wiener deconvolution demonstrates the better performance of the quaternion filter on the multicomponent traces compared to the scalar filters. Wavefield separation by means of quaternion SVD makes it possible to discern body waves from surface waves based on their different polarization characteristics and eventually leads to their effective separation.

Key words: seismic data processing, velocity analysis, deconvolution, seismic wavefield separation.

1. Introduction

With the advent of multicomponent seismology the volume of data to be processed increases, thus causing a proportional increase in the effort needed to perform the different processing steps. Even if multicomponent data carry a vectorial information, they are often processed component wise, i.e., each component per time. We propose, instead, a multicomponent approach which considers the vectorial nature of the wavefield, by introducing a quaternion algebra analysis.

Quaternions constitute an extension of the complex numbers to the hypercomplex domain. They were first introduced by Hamilton (1844) and they have an important role in physics, in which hypercomplex algebra is used for fundamental formulations of quantum mechanics (Adler, 1995). In the applied sciences, quaternions are used to compactly represent spatial rotations and, for this reason, they find application in computer graphics, robotics, control theory and aerospace problems.

In the field of signal processing, there are several quaternion applications: in image processing, pure quaternions are used to describe the colour components of RGB images (Sangwine, 1996). Furthermore, quaternion algebra is used to determine the direction of arrival (DOA) of polarized waves recorded by a vector-sensor array (Miron *et al*., 2006); in seismology,

due to its capability to compactly describe a multicomponent acquisition, quaternion algebra is employed to derive a sub-space method for the wavefield separation over a 3C vector-sensor array (Le Bihan and Mars, 2004).

In this paper we focus on the applications of hypercomplex algebra to exploration seismology, where quaternions can be used to concisely handle multicomponent data. In particular, we make a synthesis of the application results shown in Grandi *et al*. (2007), Sajeva *et al*. (2011), Menanno and Mazzotti (2012) for multicomponent (MC) velocity analysis, MC deconvolution and MC wavefields separation respectively. Theoretical developments and demostrations, which can be found in such papers, are not discussed here.

2. Brief introduction to quaternions

Quaternions are hypercomplex numbers, i.e., numbers with three imaginary components. They can be written as:

$$q = a + ib + jc + kd \tag{1}$$

where *a, b, c, d* are real numbers, and *i, j,* and *k* are imaginary units. The imaginary units satisfy the multiplication rules:

$$\begin{aligned} ij &= -ji = k \\ jk &= -kj = i \\ ki &= -ik = j \\ ii &= jj = kk = -1 \end{aligned} \tag{2}$$

It follows that quaternion multiplication is not commutative. The hypercomplex conjugate and the quaternion norm can be defined analogously to the complex domain:

$$\overline{q} = a - ib - jc - kd \tag{3}$$

$$|q| = \sqrt{\overline{q}q} = \sqrt{q\overline{q}} = \sqrt{a^2 + b^2 + c^2 + d^2} \tag{4}$$

More exhaustive description of the mathematical properties of quaternions can be found in Sudbery (1979) and Zhang (1997).

Quaternions can be conveniently used in seismic multicomponent data analysis, in fact, due to their hypercomplex formulation, they are especially apt to represent up to four data components. An example of four component acquisition is a 4C-OBC (4 Component Ocean Bottom Cable) survey, in which each receiver station is constituted by a hydrophone and a triaxial geophone, placed on the sea floor. In a quaternion representation, the hydrophone recording is

associated with the real part of the quaternion, while the geophone recordings with the imaginary parts. 3C land acquisitions can be represented as well by means of quaternions, simply neglecting the real part of the quaternion signal, i.e., by putting a=0 in Eq. (1).

As an example, let us consider a shot gather. If we denote $p_i(t)$ the time series representing the pressure recorded on the i-th hydrophone and $x_i(t)$, $y_i(t)$, and $z_i(t)$ respectively the three time series representing the x, y, and z components of the signal on the i-th geophone, then we can define a quaternion time series, such as:

$$q_i(t) = p_i(t) + ix_i(t) + jy_i(t) + kz_i(t) \tag{5}$$

Similarly we can define a pure quaternion time series:

$$q_i(t) = ix_i(t) + jy_i(t) + kz_j(t) \tag{6}$$

in case that the hydrophone recording is not of interest or not available.

The set of quaternion time series for each recording station constitutes a quaternion matrix which represents the entire input dataset.

3. Application to real data

We focus on the applications of quaternion analysis to exploration seismology, where many of the processing steps can be extended to quaternions in order to concisely handle multicomponent data. In the following, three examples are explained in some details.

4. Quaternion velocity analysis

Grandi *et al*. (2004, 2005) proposed a method for velocity analysis applicable to 2C data: they added in quadrature vertical and horizontal components, and they computed complex coherency functionals along given traveltime curves on the data trace gathers. These functionals are based on the decomposition into eigenstructures of the spatial covariance matrix (Key and Smithson, 1990), and on the approximate a priori knowledge of the propagating wavelet (Spagnolini *et al*., 1993; Grion *et al*., 1998). By means of this procedure velocity trends related to different wave types in a single velocity panel can be built.

However, this approach considers only two displacement components and discards the information that the hydrophone can bring in, when dealing with ocean bottom cable (OBC) data. To overcome this limitation, Grandi *et al*. (2007) proposed the introduction of quaternion algebra in the velocity analysis phase. In this paper, we investigate the quaternion implementation of one of the simplest coherency functionals, namely the semblance (Neidell and Taner, 1971), applied to the triaxial recording of a 2D multicomponent OBC acquisition. The data are at an early step of processing, with few operations applied, such as first-break muting, band-pass filtering and notch filtering. No attempts to match the frequency content of the various components have been tried and only a simple automatic amplitude gain has been applied to the data. Torsional modes and mud rolls have been partly attenuated by the notch filter.

Figs. 1, 2, and 3 show respectively the *x, y*, and *z* components of the CDP used for the velocity analysis. Note that the data quality is rather different among the three components: events on the *x* gather are more continuous than on the other gathers. Random and coherent noise contaminate all components and shear energy is dominant in geophone recordings. In the *z* gather (Fig. 3), it is possible to identify some P-wave reflections, such as the event at 1.85 s annotated with yellow arrows, and traces of C-wave reflections, indicated by red arrows. Differently, both *x* and *y* gathers (Figs. 1 and 2) are strongly affected by shear energy, which hides possible P reflections.

Fig. 4 shows the results of both single component and quaternion velocity analysis. The analysis carried out separately on each component produces unfocused results and evidences single velocity trends, that is, converted wave trends on *x* and *y* gathers and P-wave trend on *z* gather. The quaternion analysis, instead, simultaneously gives the velocity trends of the various wave phases and produces a better focused velocity panel.

5. Quaternion deconvolution

Few attempts at vectorial multicomponent deconvolution exist. For instance, the design of multichannel deconvolution (Treitel, 1970) can be extended to the multicomponent case, as indicated by Claerbout (1985); in this approach, the multichannel filtering operation is represented as a linear system. A similar solution consists in concatenating each component time series into a long vector and then to process the resulting record as a single component. Anderson and Nehorai (1996), and Menanno and Le Bihan (2010) applied this procedure to vector-sensor acquisitions.

A quaternion formulation of deconvolution has been proposed for the first time by Menanno and Mazzotti (2012). They compare scalar and quaternion deconvolution in synthetic and real data examples, and they show that quaternion deconvolution provides a better wavelet estimation and thus an improved deconvolution performance.

In this paper, we consider the application of quaternion spiking deconvolution to a real common receiver gather pertaining to an OBC multicomponent acquisition. A portion of the multi-component gather before the application of spiking deconvolution is shown in Fig. 5; the *x, y*, and *z* components are shown respectively in the (a), (b), and (c) panels. The data have undergone a limited pre-processing that consists of 3-C amplitude balancing, first-break muting and band-pass filtering to attenuate the torsional modes that affect all the recordings.

In the frame of the *z* component (Fig. 5c), a compressional event is clearly visible at approximately 1.9 s, and it is marked with a red arrow; its pegleg, which is pointed to by a second red arrow, follows with a delay of ≈ 0.15 s. Note that these events are also visible with lower amplitudes on the horizontal components. Furthermore a residual coherent noise, due to torsional modes, affects all the gathers, particularly at near offset. On the horizontal gathers this noise is stronger than the compressional event, while it is weaker on the vertical one.

The results of scalar and quaternion deconvolutions are shown in Figs. 6a, 6b, and 6c and Figs. 7a, 7b, and 7c. For both deconvolutions the operator parameters are: filter length = 80 ms, prewhitening = 0.1%, and both operators are computed on a 1s long time window, which mainly contains compressional energy. In figures, the red arrows point to the compressional event, and the blue arrows indicates the coherent noise, which still affects the horizontal components after

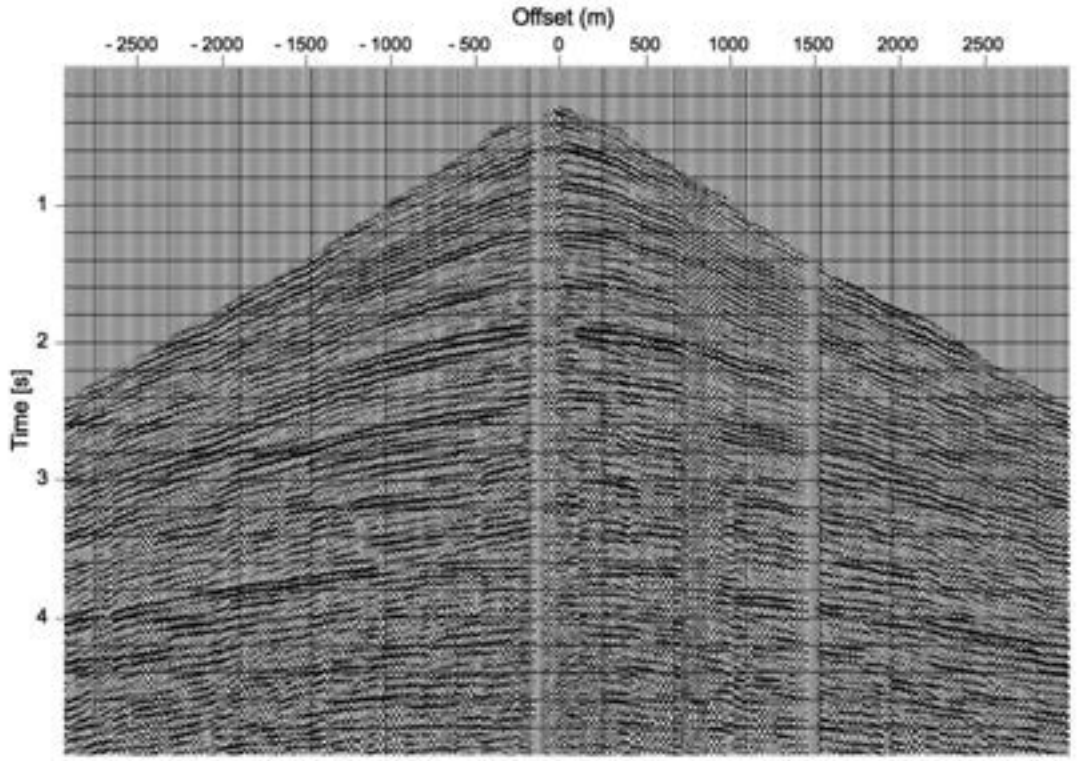

Fig. 1 - CDP *x* component of the data from an OBC acquisition.

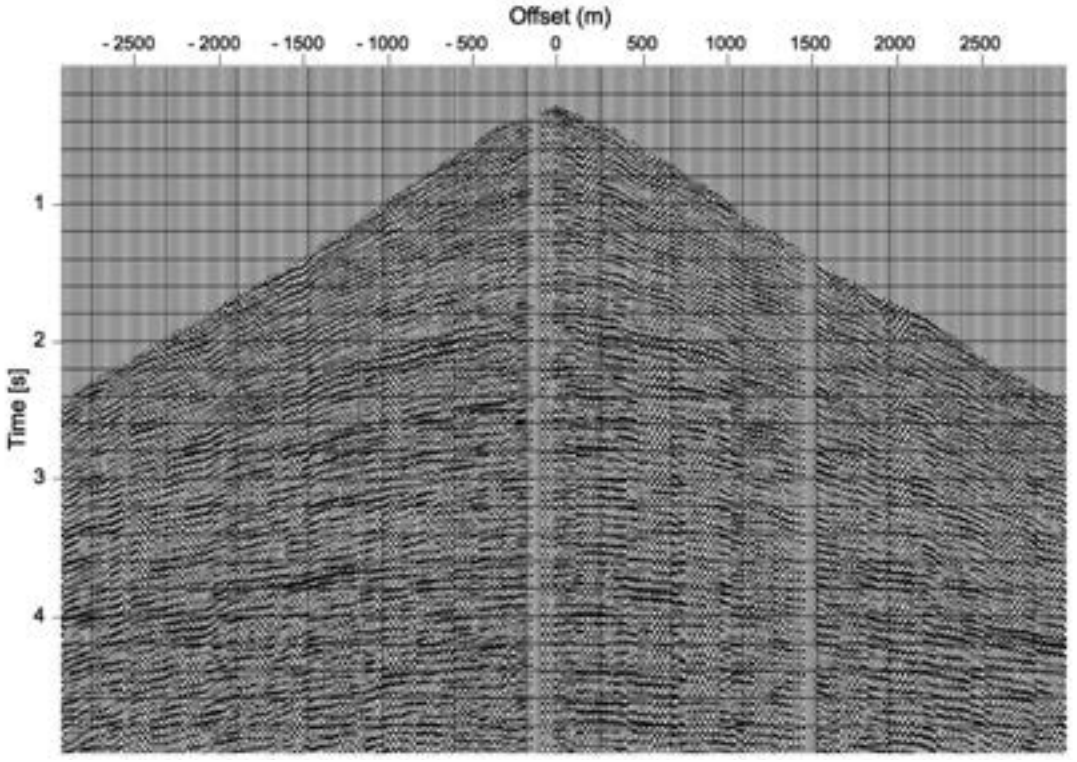

Fig. 2 - CDP *y* component of the data from an OBC acquisition.

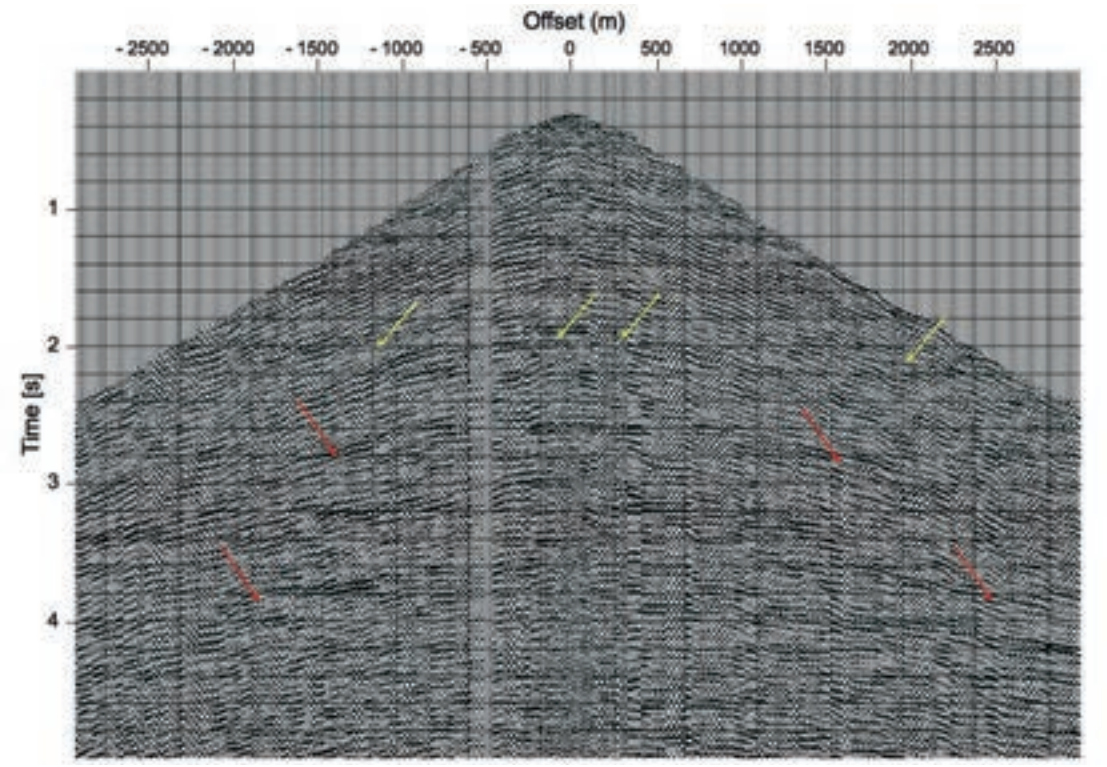

Fig. 3 - CDP *z* component of the data from an OBC acquisition.

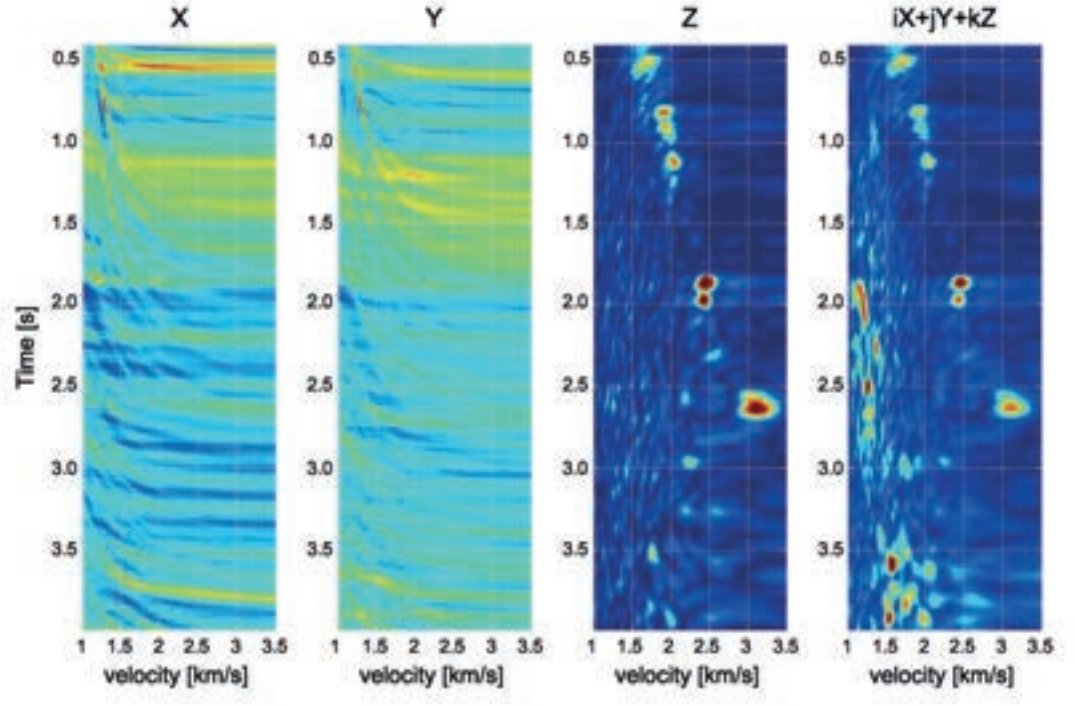

Fig. 4 - Semblance velocity panels: single component semblance for the *x, y*, and *z* components, and quaternion semblance.

deconvolution.

The quaternion deconvolution, recognizing the vectorial nature of the signal, emphasizes the compressional event in the quaternion space. This is apparent on the horizontal projections of the quaternion output (Figs. 7a and 7b) where the compressional event stands out more clearly with respect to the standard deconvolution outputs (Figs. 6a and 6b). Finally, the quaternion deconvolution seems also to perform better in the attenuation of the torsional modes, the hyperbolic-like coherent noise pointed to by the blue arrows and evident at short offsets.

6. Quaternion seismic wavefield separation

Another important topic in seismology is the separation of surface and body wavefields. In particular, we consider the extraction of a single Rayleigh wave mode from a multicomponent land data set, leaving as a residual the body wavefield, other surface waves, and noise. In the following, we show and discuss the results of the application of the procedure described in (Sajeva *et al*., 2011).

The data are shown in Fig. 8 in three different domains: (a) offset-time, (b) inverse ellipticity-offset, and (c) frequency-ray parameter (*f-p* domain), and, on each panel, the Rayleigh wave mode is labeled with *RW* letters. Both (a) and (c) show the *z* component only (the behavior of the *x* component is analogous to the *z* compoment, while the *y* component is negligible), and (b) is computed on the *x-z* plane.

In the time offset domain (Fig. 8a) the Rayleigh wave mode consists in the slowest wave train, and it has a reverse funnel shape caused by frequency dispersion. In the inverse ellipticity-offset map (Fig. 8b) the z component has been 90 degree phase shifted before the computation of the inverse ellipticity. This permits to collapse circular polarization and elliptic polarization with any eccentricity to linear polarization. In fact, recalling that the inverse ellipticity map plots the ratio of the first two eigenvalues (σ_2/σ_1) computed on portions of the data (containing the *x* component and the 90 degree phase shifted z component in this case), the Rayleigh wave has $\sigma_2=0$ (linear polarization), and inverse ellipticity ($\sigma_2/\sigma_1=0$). At the opposite, incoherent noise is not affected by the phase shift, then $\sigma_1=\sigma_2$ and its inverse ellipticity equals one. This trick allows us to visually distinguish incoherent noise from elliptically polarized signals (Rayleigh waves). In this domain, the Rayleigh wave mode corresponds to a blue zone (zero), which is indeed clearly visible in the map (Fig. 8b). In the *f-p* domain (Fig. 8c), we identify the mode with the broken curve composed by three branches with values ranging from 3.5 to 5.8 ms/m pointed by the arrow in the figure. The curve has the ray parameter varying with frequency, i.e., it is a frequency dispersive signal.

The extraction method has been implemented both on the *x, y, z* components separately and with a quaternion representation, the results (the extracted modes) are shown in Figs. 9 and 10. Comparing the original data with the extracted modes, we expect them to be approximately equal where the mode is dominating, and to differ elsewhere.

Using the single component implementation (Fig. 9): in the offset time domain (Fig. 9a), the faster signals (body waves, other surface waves) are correctly attenuated, however, also part of the Rayleigh wave mode is attenuated; in the inverse ellipticity-offset domain (Fig. 9b), the Rayleigh wave zone has values ranging from 1 to 0, and a clear elliptic zone (blue) cannot be recognized; in the *f-p* domain (Fig. 9c), the dispersion curve of the mode is affected by the same attenuation

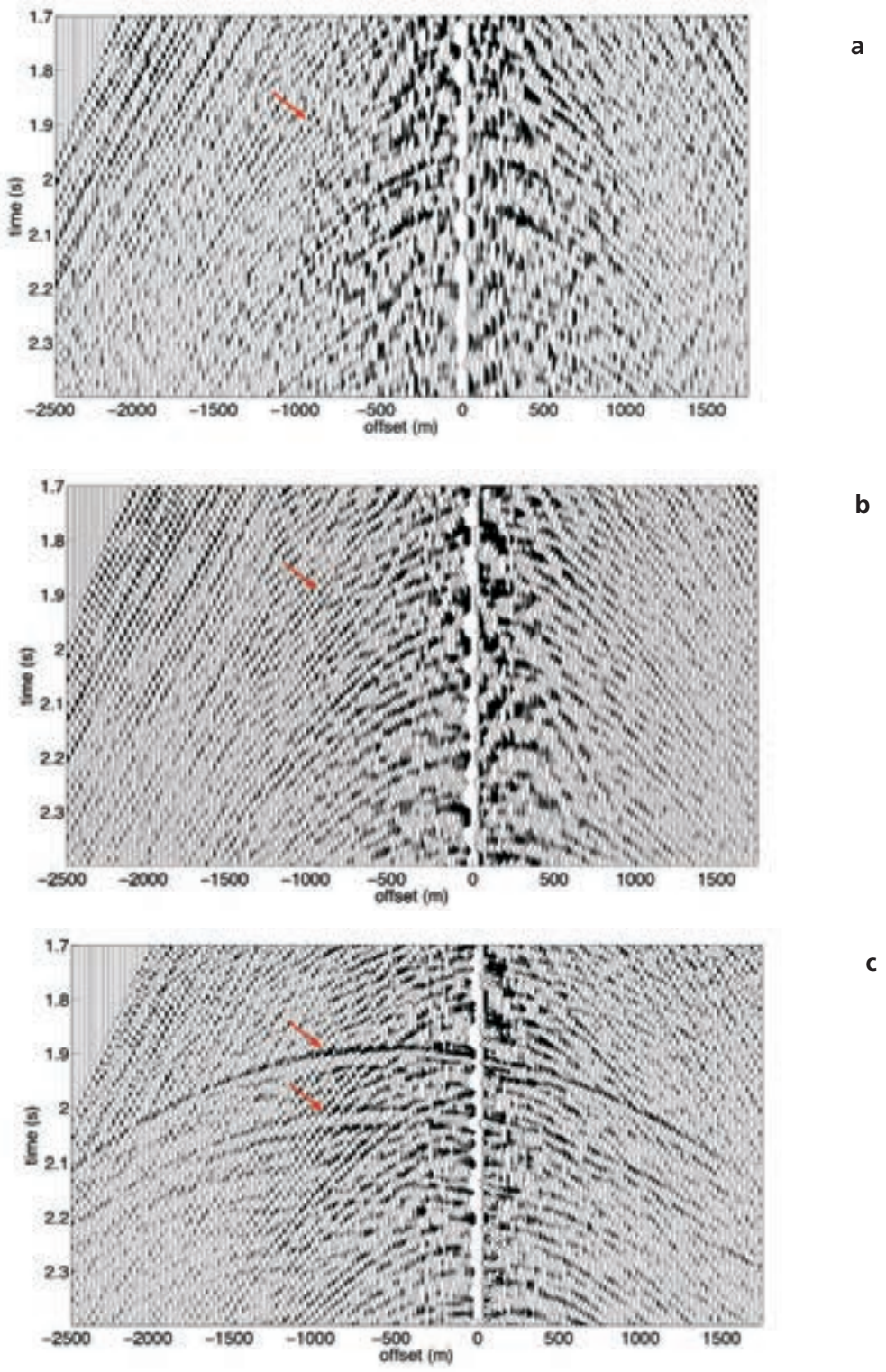

Fig. 5 - A portion of the gather: *x* component (a); *y* component (b); *z* component (c). Red arrows point to the compressional events, which are clearly visible on the *z* component and barely visible on the *x* and *y* components.

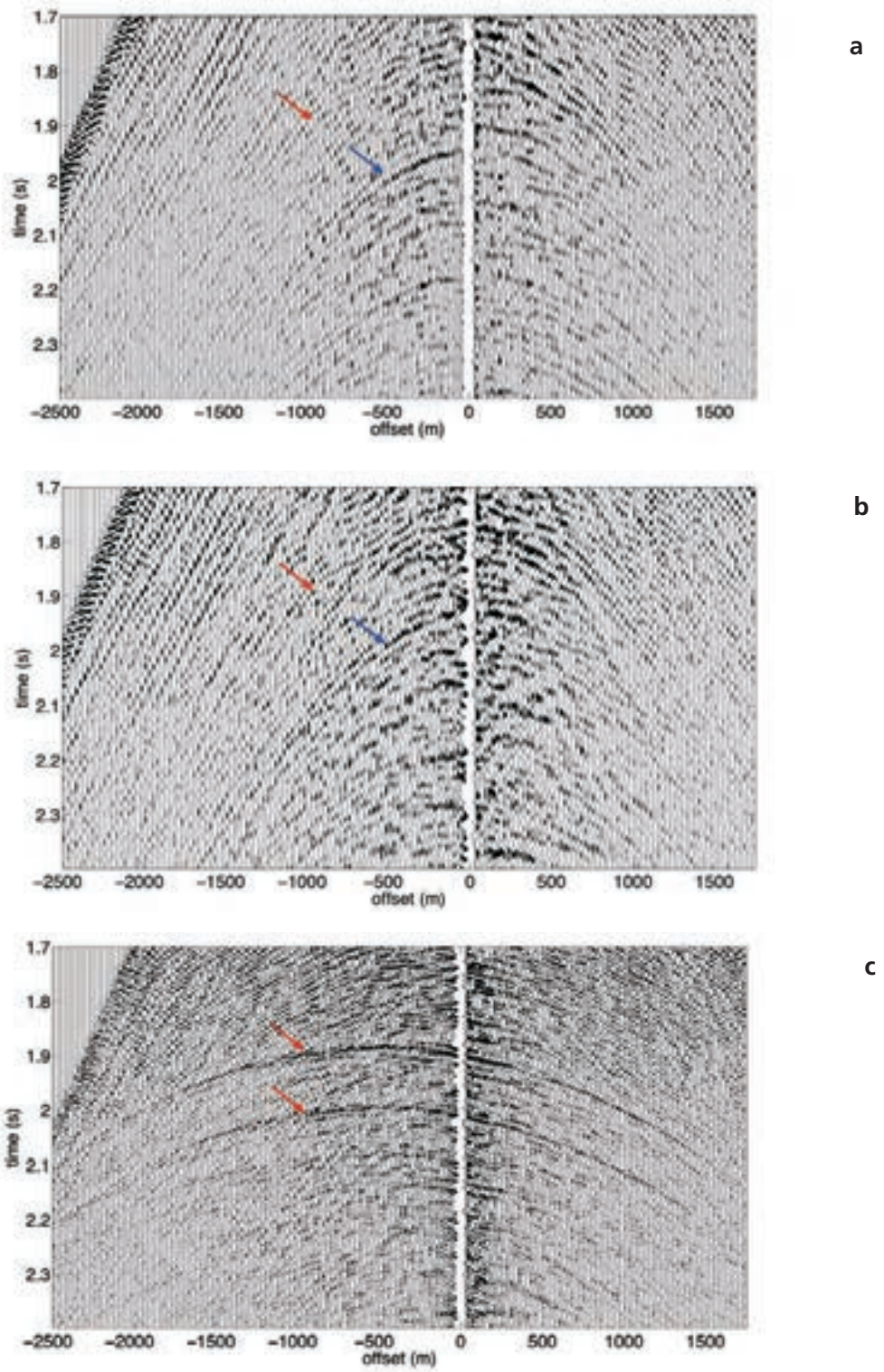

Fig. 6 - The portion of the gather after single component spiking deconvolution: *x* component (a); *y* component (b); *z* component (c). Red arrows point to the compressional events, and blue arrows indicate the torsional mode coherent noise.

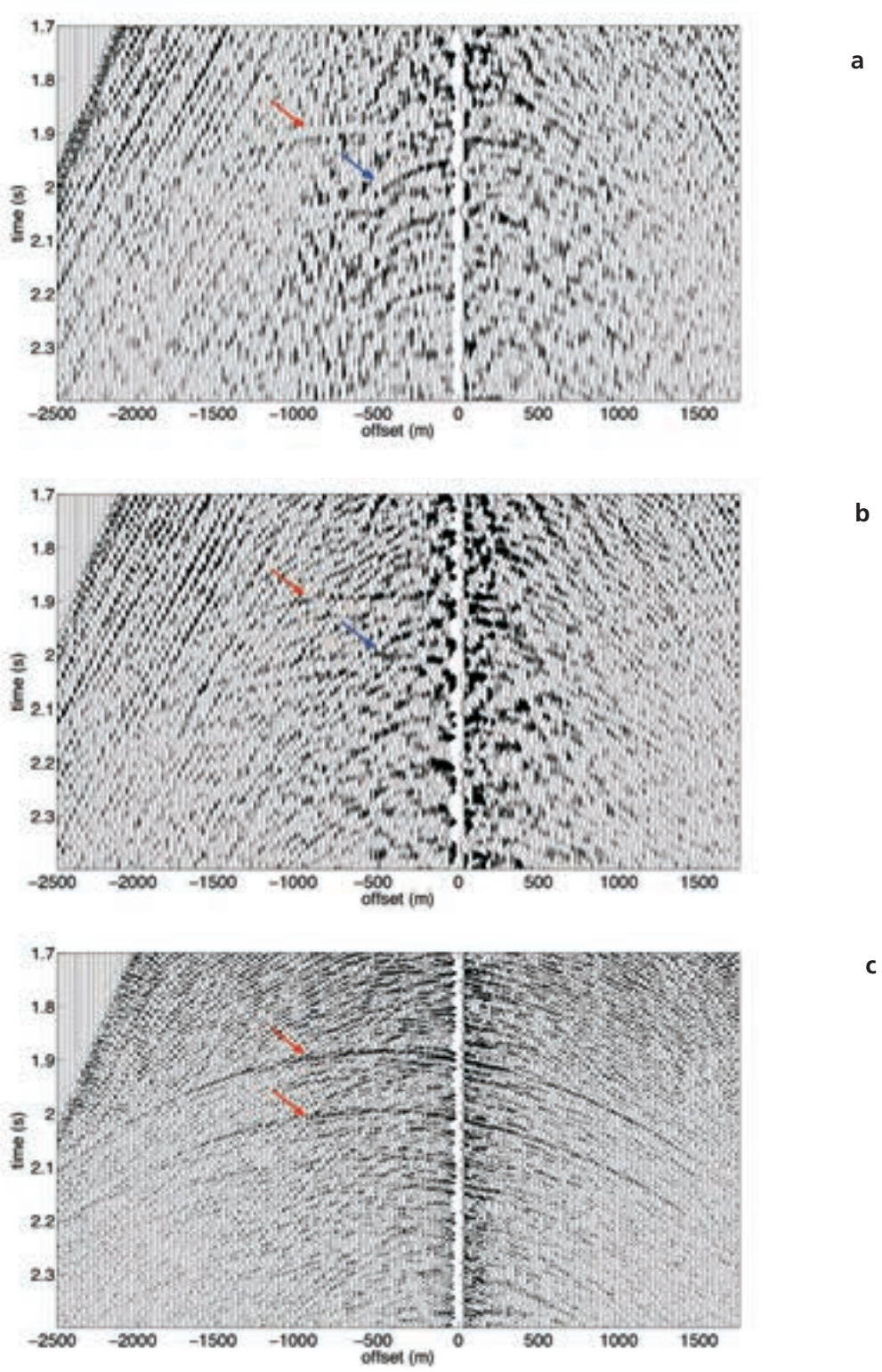

Fig. 7 - The portion of the gather after quaternion spiking deconvolution: *x* component (a); *y* component (b); *z* component (c). Red arrows point to the compressional events, and blue arrows indicate the torsional mode coherent noise.

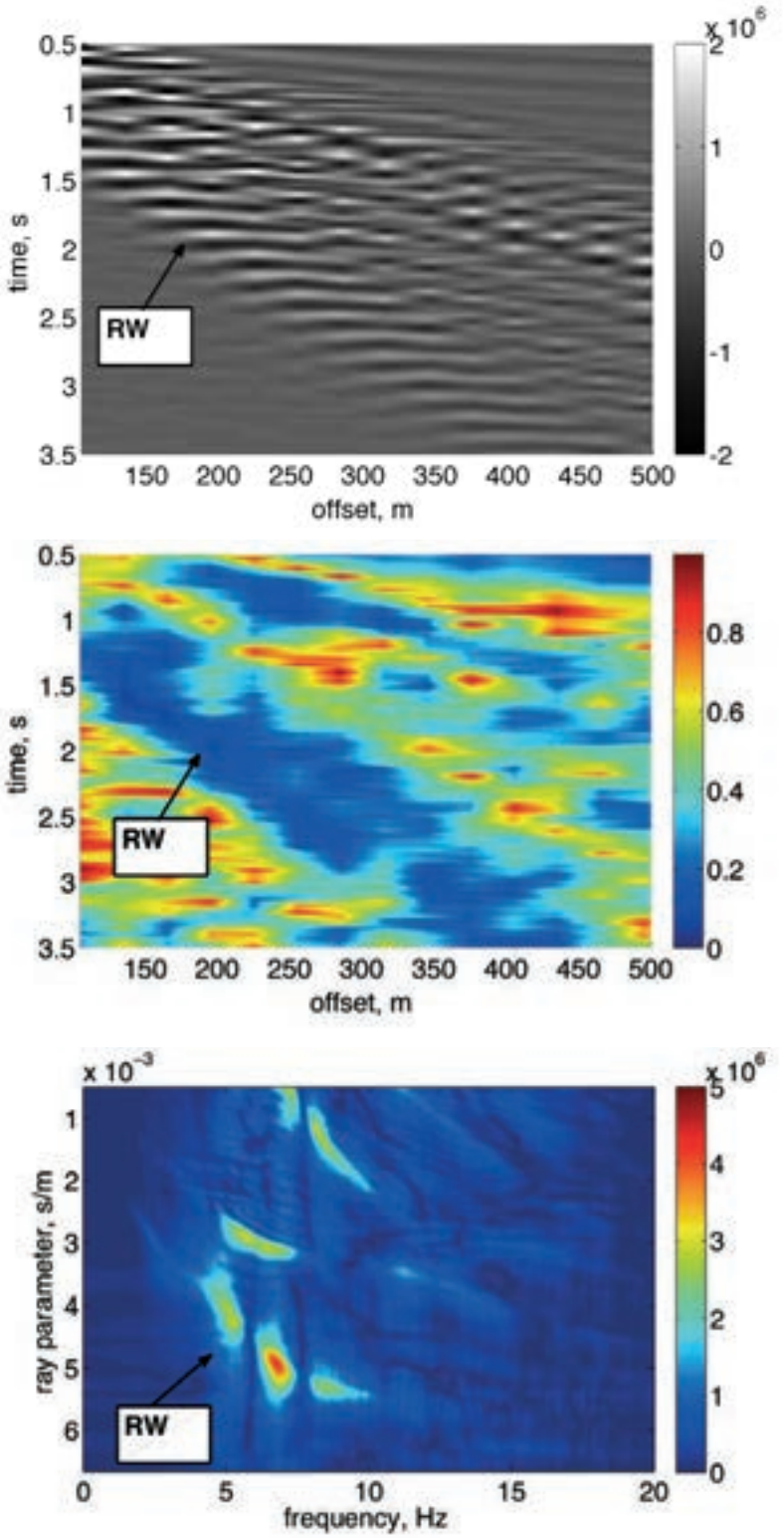

Fig. 8 - The original dataset: the *z* component in the offset-time domain (a); the inverse ellipticity-offset map in the *x*-*z* plane after a 90 degree phase shift of the *z* component (b); the *z* component in the frequency-ray parameter domain (c). In the graphs, the RW label points out the Rayleigh Wave mode to be extracted.

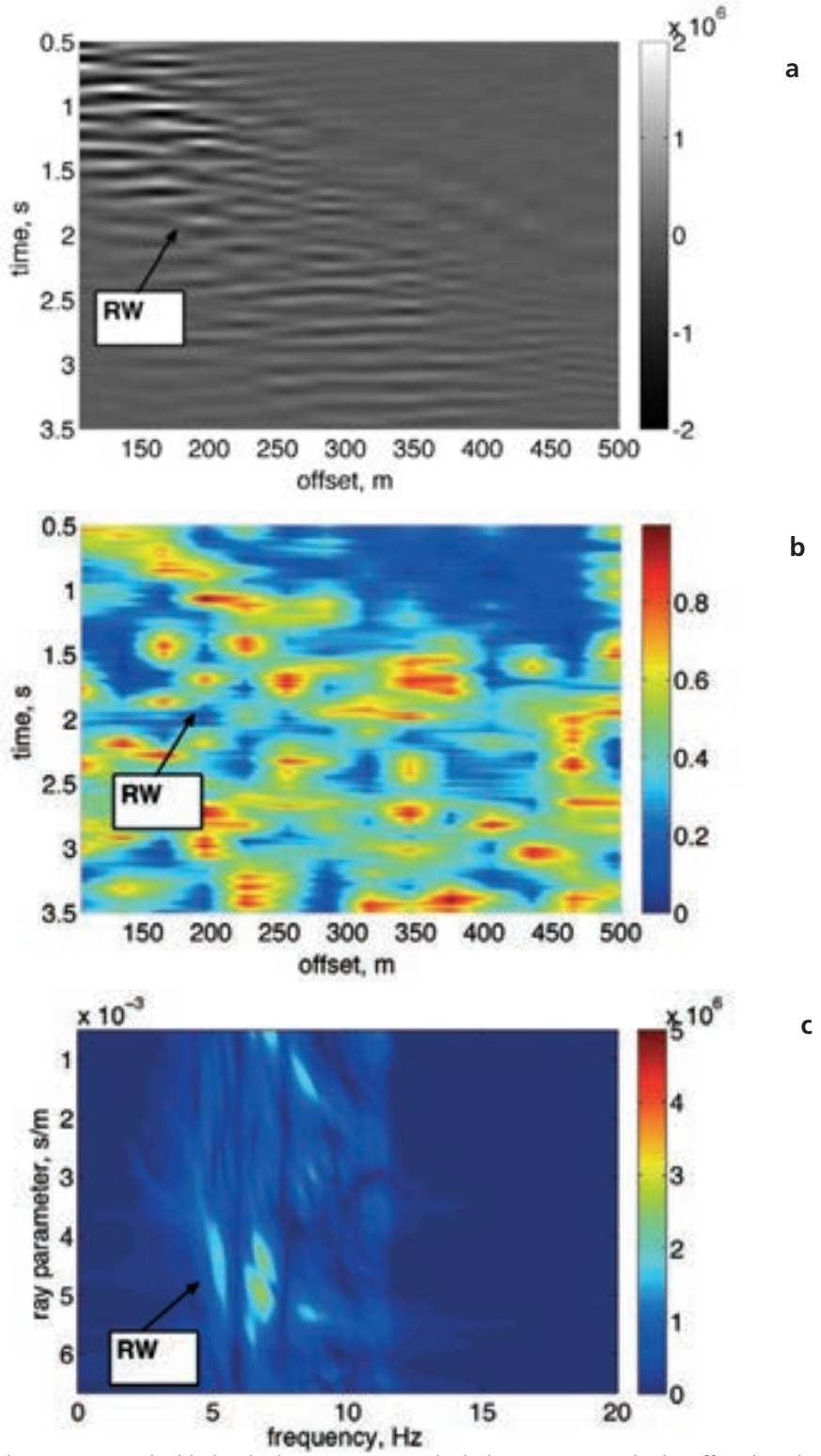

Fig. 9 - The Rayleigh wave extracted with the single component method: the *z* component in the offset-time domain (a); the inverse ellipticity-offset map in the *x*-*z* plane after a 90 degree phase shift of the *z* component (b); the *z* component in the frequency-ray parameter domain (c). In the graphs, the *RW* label points out the extracted Rayleigh Wave mode.

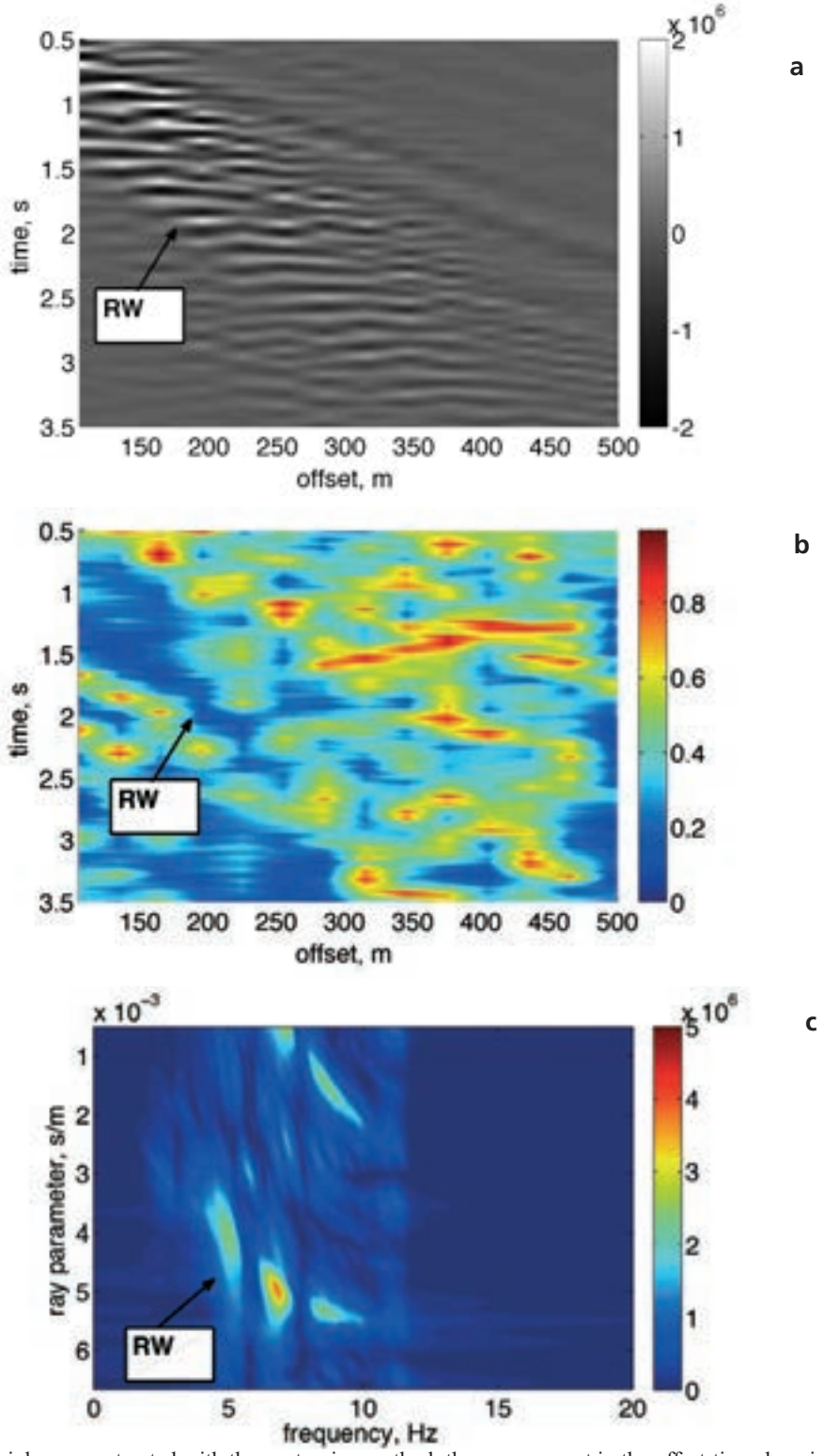

Fig. 10 - The Rayleigh wave extracted with the quaternion method: the *z* component in the offset-time domain (a); the inverse ellipticity-offset map in the *x*-*z* plane after a 90 degree phase shift of the *z* component (b); the *z* component in the frequency-ray parameter domain (c). In the graphs, the *RW* label points out the extracted Rayleigh Wave mode.

present in (Fig. 9a).

Using the quaternion implementation (Fig. 10): in the offset time domain (Fig. 10a) the energy of the mode is better preserved along the offset; in the polarization map (Fig. 10b) a blue zone is present in the offset range 0-200 m, instead for longer offsets inverse ellipticity assumes values mainly in the range 0-0.6 and, as previously, a clear elliptic zone cannot be recognized; in the *f-p* domain (Fig. 10c), the dispersion curve of the mode is visible and most part of its energy is preserved.

In conclusion, the quaternion implementation shows an improvement with respect to the single component implementation on each of the three different domains: offset-time, inverse ellipticity-offset, and *f-p* domains.

7. Conclusions

The very nature of quaternions, hypercomplex numbers, makes them perfectly suited to treat multicomponent seismic data and to honour the vectorial nature of the incoming wave fields. In particular, quaternion velocity analysis simultaneously evidences velocity trends pertaining to different wave modes, and it helps the interpreter to estimate interval V_p and V_s by means of event correlation, and to correlate information between VSP and well logs. Moreover, it speeds up the velocity picking, which can be performed in a single pass on a multicomponent velocity panel, rather than once for each single velocity panel.

Analogously, quaternion deconvolution performs superiorly than single component deconvolution, taking advantage of the signal that is simultaneously present in all the components.

Finally, the results of the quaternion extraction of Rayleigh waves show a better performance with respect to single component algorithms for both polarization and lateral continuity properties; this is explained by the ability of quaternions to compactly represent elliptically polarized signals.

This overview of recently achieved research results, which have been separately published, suggests the chance of extending the quaternion approach to other steps of seismic processing, and eventually to perform a complete quaternion processing sequence for multicomponent data.

REFERENCES

Adler S.; 1995: *Quaternionic quantum mechanics and quantum fields*. Oxford University Press, 586 pp.

Anderson S. and Nehorai A.; 1996: *Analysis of a polarized seismic wave model.* IEEE Trans. Signal Process., **44**, 379-386.

Claerbout J.; 1985: *Fundamentals of geophysical data processing with applications to petroleum prospecting.* Blackwell Scientific Publications, Palo Alto, CA, USA, 274 pp.

Grandi A., Mazzotti A. and Stucchi E.; 2007: *Multicomponent velocity analysis with quaternions.* Geophys. Prospect., **55**, 761-777.

Grandi A., Stucchi E. and Mazzotti A.; 2004: *Multicomponent velocity analysis by means of covariance measures and complex matched filters.* In: Proc. 74th SEG Meeting, Denver, CO, Texas, USA, Expanded Abstract, pp. 2415-2418.

Grandi A., Stucchi E. and Mazzotti A.; 2005: *V_p/V_s Ratios through multicomponent velocity analysis.* In: Proc. 67th

EAGE Conf., Madrid, Spain, Expanded Abstract, pp. B024 1-24.

Grion S., Mazzotti A. and Spagnolini U.; 1998: *Joint estimation of AVO and kinematic parameters.* Geophys. Prospect., **46**, 405-422.

Hamilton W.R.; 1844: *On quaternions: or a new system of imaginaries in algebra.* The Philosophical Magazine, 3rd series, **25**, 489-495.

Key S.C. and Smithson S.B.; 1990: *New approach to seismic-reflection event detection and velocity determination.* Geophsics, **55**, 1057-1069.

Le Bihan N. and Mars J.; 2004: *Singular value decomposition of quaternion matrices: a new tool for vector-sensor signal processing.* Signal Process., **84**, 1177-1199.

Menanno G. and Le Bihan N.; 2010: *Quaternion polynomial matrix diagonalization for the separation of polarized convolutive mixture.* Signal Process., **90**, 2219-2231.

Menanno G. and Mazzotti A.; 2012: *Deconvolution of multicomponent seismic data by means of quaternions: theory and preliminary results.* Geophys. Prospect., **60**, 217-238.

Miron S., Le Bihan N. and Mars J.; 2006: *Quaternion-MUSIC for vector-sensor array processing.* IEEE Trans. Signal Process., **54**, 1218-1229.

Neidell N.S. and Taner M.T.; 1971: *Semblance and other coherency measures for multichannel data.* Geophsics, **36**, 482-497.

Sajeva A., Menanno G.M. and Mazzotti A.; 2011: *Modal identification and extraction of Rayleigh waves by means of quaternion SVD and group velocity curves.* In: Proc. 73rd EAGE Conference & Exhibition Wien, Austria, pp. P095 1-4.

Sangwine S.; 1996: *Fourier transforms of colour images using quaternion, or hypercomplex numbers.* Electron. Lett., **32**, 1979-1980.

Spagnolini U., Macciotta L. and Manni A.; 1993: *Velocity analysis by truncated singular value decomposition.* In: Proc. 63rd SEG Meeting, Washington, DC, USA, pp. 677-680.

Sudbery A.; 1979: *Quaternionic analysis.* Math. Proc. Camb. Phil. Soc., **85**, 199-225.

Treitel S.; 1970: *Principles of digital multichannel filtering.* Geophys., **35**, 785-811.

Zhang F.; 1997: *Quaternion and matrices of quaternions.* Linear Algebra and its Applications, **251**, 21-57.

Corresponding author: Alfredo Mazzotti
Earth Sciences Department, University of Pisa
Via Santa Maria 53, 56126 Pisa, Italy
Phone: +39 050 2215794; fax: +39 050 2215800; e-mail: mazzotti@dst.unipi.it